

Soliton Squeezing in a Mach-Zehnder Fiber Interferometer

Marco Fiorentino, Jay E. Sharping, and Prem Kumar

Center for Photonic Communication and Computing, Department of Electrical and Computer Engineering, Northwestern University, 2145 N. Sheridan Road, Evanston, IL 60208-3118, USA

Dmitry Levandovsky

Tellabs Operations Inc., 4951 Indiana Ave., Lisle, IL 60532, USA

Michael Vasilyev

Corning Inc., 2200 Cottontail Lane, Sommerset, NJ 08873, USA

A new scheme for generating amplitude squeezed light by means of soliton self-phase modulation is experimentally demonstrated. By injecting 180-fs pulses into an equivalent Mach-Zehnder fiber interferometer, a maximum noise reduction of 4.4 ± 0.3 dB is obtained (6.3 ± 0.6 dB when corrected for losses). The dependence of noise reduction on the interferometer splitting ratio and fiber length is studied in detail.

Current interest in efficient generation of squeezed radiation in optical-fiber devices is prompted by the possibility of using the resulting highly-squeezed fields to create and distribute continuous-variable entanglement for quantum-communication applications such as teleportation and dense coding [1]. Several schemes to generate amplitude-squeezed light by use of the Kerr nonlinearity in optical fibers have recently been devised [2–6]. The most successful soliton amplitude-squeezing experiments to date have used an asymmetric Sagnac interferometer, leading to 3.9 dB (6.0 dB when corrected for losses) [3] and 5.7 dB (6.2 dB when corrected for losses) [5] of noise reduction, respectively. As shown schematically in Fig. 1, the amplitude squeezing in such experiments results from the combined effect of soliton’s nonlinear propagation in the fiber and its subsequent mixing with an auxiliary weak pulse at the fiber output. The mixing rotates the total mean field relative to the soliton’s noise, which gets shaped into a “crescent” through the nonlinear interaction, thus allowing the squeezing to be measured in direct detection. To obtain a high degree of noise reduction, it is then crucial to control the relative amplitude and phase of the two pulses. In the Sagnac configuration [3,5] the pulses counter propagate in the same fiber, thus preventing the control of their relative phase. Moreover, the relative amplitude between the soliton-like pulse and the auxiliary dispersive pulse is unchangeable once one fixes the splitting ratio of the interferometer beamsplitter.

To overcome these drawbacks we investigate the setup shown in Fig. 2. In this rendition, the Sagnac geometry

is “unfolded” into a polarization Mach-Zehnder formed between two polarization beam splitters, PBS2 and PBS3, wherein the two arms of the interferometer correspond to the two polarization modes of a single-mode polarization-maintaining (PM) fiber (3M-FSPM 7811). The Mach-Zehnder geometry allows independent control of the phase and amplitude of the auxiliary pulse relative to the soliton. By adding these new degrees of freedom, we are able to study in greater detail the physical process that leads to noise reduction.

In our setup the light source is a tunable optical-parametric oscillator (Coherent Inc., model Mira-OPO) emitting a train of pulses at a wavelength of 1538 nm with a 75 MHz repetition rate and 180 fs (FWHM) pulse width. The pulses are *sech* shaped and nearly Fourier transform limited (time-bandwidth product $\simeq 0.4$). The source is used to inject one arm of the interferometer with a strong pulse, propagating in the soliton regime, and the other with a weak, dispersive pulse ($\simeq 10\%$ of the fundamental soliton energy). The total injected power and the relative powers of the two pulses are controlled by using a half-wave plate (HWP1) and a polarizing beamsplitter (PBS1). Since the pulses propagate with significantly different group velocities in the two polarization modes, they are launched at different times into the fiber in order for them to overlap at the fiber output. The relative delay is introduced by adding separate free-space propagation paths [$s(p)$ -polarization reflects from M1 (M2)] for the two polarization modes in the interferometer. This arrangement also prevents cross interaction between the two pulses, as they are temporally separated during most of the propagation distance in the fiber. In addition, a piezoelectric control on M1 allows fine tuning of the relative phase between the pulses. A half-wave plate (HWP2) and a quarter-wave plate (QWP3) are used to inject the s and p polarized pulses from free space into the correct polarization modes of the fiber.¹ At the output of the fiber, the two pulses are recombined using a half-wave plate (HWP3) and a polarizing beamsplitter (PBS3), allowing us to easily change the recombination ratio T (defined as the ratio of powers of the weak to the strong pulse reflected by PBS3) by turning HWP3. The combined pulse, reflected by PBS3, is reflected off another polarization

¹In principle QWP3 shouldn’t be necessary, but we found that it greatly improves the polarization purity of the pulses at the fiber output. This, perhaps, is due to the fact that the polarization eigenmodes of the PM fiber are not exactly linearly polarized.

beamsplitter (PBS4) in order to insure a high polarization purity while minimizing optical losses. The emerging 75MHz pulse train is then analyzed with a four-diode balanced detector, wherein four photodiodes (Epitaxx ETX500) are used to increase the saturation power to 40 mW of average power. To increase the overall detection efficiency, we use spherical mirrors that bounce back the light reflected from the photodiode surfaces. This configuration yields a total measured detection efficiency of 78%, where the Fresnel loss at the fiber end (5%), propagation losses through various optical elements (8%), and sub-unity photodetector quantum efficiencies (equivalent losses of 11%) are the contributing factors. For better squeezing measurements, the Fresnel loss was also mitigated by using a window that is anti-reflection coated on one side. The uncoated side is put in optical contact with the uncoated fiber tip using an index-matching gel (Nye Lubricants OC-431A-LVP). We estimate that this improves the overall detection efficiency to 82%.

The experimental results are shown in Fig. 3. We study the quantum-noise reduction in the photocurrent spectral density at 28.7MHz as a function of the average optical power which is proportional to the squared soliton number N^2 in the soliton arm of the interferometer. Figures 3(a)–(c) illustrate the quantum-noise reduction for fiber lengths of 3.4, 6, and 9 m, corresponding to 2.5, 4.3, and 6.5 soliton periods, respectively. The noise reduction was maximized by adjusting the relative phase between the pulses in the interferometer arms. Data sets represented by filled circles refer to the maximum noise reduction, which is obtained with T equal to: (a) $(0.4 \pm 0.1)\%$, (b) $(0.32 \pm 0.01)\%$, and (c) $(0.53 \pm 0.05)\%$, respectively. The best noise reductions measured are: (4.1 ± 0.3) dB for the setup with 78% detection efficiency and (4.4 ± 0.3) dB for that with 82% detection efficiency. These correspond respectively to (6.3 ± 0.6) dB and (6.6 ± 0.7) dB of inferred noise reduction at the fiber output when degradations due to linear losses are taken into account.

The data in Fig. 3 clearly show a pronounced dependence of the noise reduction on the recombination ratio T , the fiber length, and the input average power. The analysis of such dependencies requires a model for the propagation of the pulses' quantum noise in the fiber. An analytical solution for the propagation of the quantum noise of the fundamental soliton ($N = 1$) and the associated continuum is possible [7,9,10]. This analytical solution has been

applied to the analysis of squeezing experiments that use interferometers [10]. We show the comparison of this latter analysis with our experimental data in the inset of Fig. 4(a), where only the points with $N = 1$ are plotted. However, when the pulses are not fundamental solitons, there is no known analytical solution for the propagation of the quantum noise. Several works have applied numerical methods to solve this problem and such numerical solutions have been used to analyze the noise-reduction properties of asymmetric Sagnac interferometers [3,12]. A common feature of all of these works is that the calculated noise reduction exceeds, by a sizable amount, any experimental result obtained so far. Remarkably, however, the theory seems to be able to reproduce the overall structure of the experimental data.

In our analysis, we have focused on the features of quantum-noise reduction vs. average power and the associated dependence on the recombination ratio. To do this, we have performed a numerical simulation of the Mach-Zehnder interferometer. At the core of the simulation is a routine that propagates quantum noise through the fiber. This routine relies on the standard linearization technique [13] for solving the quantum nonlinear Schrödinger equation (NLSE)

$$\frac{\partial \hat{U}}{\partial z} = i\hat{U}^\dagger \hat{U} \hat{U} + \frac{i}{2} \frac{\partial^2 \hat{U}}{\partial t^2}, \quad (1)$$

which describes the evolution of the annihilation operators \hat{U} for the envelope of the electric field in the fiber. Equation (1) is written in a retarded frame moving together with the pulse along z , which is expressed in standard normalized-length units [11]. We linearize this equation by putting $\hat{U} = \langle \hat{U} \rangle + \hat{u}$, where \hat{u} is the annihilation operator for the fluctuations, keeping only terms up to first order in \hat{u} . This yields a pair of coupled equations: the zeroth-order expansion represents the classical NLSE, which describes the evolution of the envelope $\langle \hat{U} \rangle$, whereas the first-order expansion gives a linear equation for the fluctuation operator \hat{u} . Applying the discretization procedure described in Ref. [12], we have developed a computer program to solve the fluctuation equation numerically, assuming that a solution (numerical or analytical) is given for the corresponding classical NLSE. Our algorithm uses a split-step Fourier method, wherein each step is solved exactly using matrix exponentiation. The behavior of the Mach-Zehnder interferometer is simulated by propagating the averaged envelopes of the soliton-like and the auxiliary pulses through

equal lengths of the fiber. Using these numerical solutions for the averaged envelopes we then propagate the noise operators for the soliton-like pulse. At the output of the interferometer, the soliton-like pulse is mixed with the auxiliary pulse. We consider two cases in our simulations: for the curves marked by hollow squares connected with a dashed line, we assume coherent-state noise for the auxiliary pulse; whereas for the curves marked by solid circles connected with a continuous line, we numerically propagate the noise of the auxiliary pulse through the fiber as well. As expected, the effect of the quantum-noise evolution of the auxiliary pulse is larger for larger recombination ratios [Fig. 4 (c)]. We attribute the oscillations in the noise reduction to phase chirp introduced by dispersion in the fiber. This also explains why the frequency of oscillations is approximately doubled, when the propagation of the auxiliary pulse in the fiber is fully taken into account.

In Fig. 4(a)–(c) we compare the results of our simulations for the 6.0 m fiber length and various recombination ratios with the corresponding experimental data sets that have been corrected for detection losses. The calculated values of noise reduction do not quantitatively agree with the experimental data, which show little evidence of the oscillations. Nevertheless, the theory correctly predicts a saturation in the detected noise reduction for large values of N^2 , which we attribute to increasing temporal mismatch in the overlap between the soliton-like and the auxiliary pulses. Reasons for the discrepancy between the theory and the experiment have been discussed in the literature with authors reaching differing conclusions. Some [3] believe the discrepancy to be due to the Raman effect (that we have found to be significant in our setup) and their claim is partially supported by papers that discuss limits on squeezing imposed by the Raman noise [14]. Other authors [15] have reported results of numerical calculations with inclusion of the Raman effect, but the results show that the Raman noise does not seem to play a significant role. Finally, the authors of one experiment [2] cooled the fiber to liquid nitrogen temperature and observed an increase in the noise reduction, thus suggesting a preeminent role for thermal phase scattering owing to guided-wave Brillouin scattering; whereas others [17] were able to achieve a good matching between the theory and data in an experiment where both Brillouin and Raman scattering were negligible. These discrepancies between the various studies suggest that further investigation, both theoretical and experimental, is warranted.

In conclusion, we have studied a Mach-Zehnder nonlinear fiber interferometer for generation of amplitude-squeezed light. By varying the key parameters of the interferometer, such as the fiber length, recombination ratio, and average input power, we optimized its performance and measured large amounts of amplitude squeezing. In addition, by using numerical analysis we have tried to understand the dependencies of noise reduction on these key parameters.

The authors thank G. Biondini for useful suggestions in the numerical simulations and E. Corndorf for his help with the computers. This work was supported in part by the U.S. Army Research Office through the MURI grant DAAD19-00-1-0177 and the associated MURI Fellowship (DAAD19-00-1-0469) for J. E. Sharping.

-
- [1] A. Furusawa, J.L. Sorensen, S. L. Braunstein, C. A. Fuchs, H. J. Kimble, and E. S. Polzik, *Science* **282**, 706 (1998); S. L. Braunstein and H. J. Kimble, *Phys. Rev. A*, **61** 2302 (2000).
 - [2] M. Rosenbluh and R. M. Shelby, *Phys. Rev. Lett.* **66**, 153 (1991).
 - [3] S. Schmitt, J. Ficker, M. Wolff, F. König, A. Sizmann, and G. Leuchs, *Phys. Rev. Lett.* **81**, 2446 (1998).
 - [4] S. Spälter, M. Burk, U Ströβner, A. Sizmann, and G. Leuchs, *Opt. Express* **2**, 77 (1998).
 - [5] D. Krylov and K. Bergman, *Opt. Lett.* **23**, 1390 (1998).
 - [6] D. Levandovsky, M. Vasilyev, and P. Kumar, *Opt. Lett.* **24**, 948 (1999)
 - [7] H.A. Haus and Y. Lai, *J. Opt. Soc. Am.* **7** 386 (1990).
 - [8] D. Levandovsky, M. Vasilyev, and P. Kumar, *Opt. Lett.* **24**, 43 (1999)
 - [9] D. J. Kaup, *Phys. Rev. A* **42**, 5689 (1990)
 - [10] D. Levandovsky, M. Vasilyev, and P. Kumar, *Opt. Lett.* **24**, 89 (1999).
 - [11] G.P. Agrawal, *Nonlinear fiber optics*, 2nd ed. San Diego (1995).
 - [12] C.R. Doerr, M. Shirasaki, and F.I. Khatri, *J. Opt. Soc. Am.*, **11**, 142 (1994).
 - [13] M. Shirasaki and H.A. Haus, *J. Opt. Soc. Am.* **7**, 30 (1990).
 - [14] J.H. Shapiro and L. Boivin, *Opt. Lett.* **20**, 925 (1990).
 - [15] M.J. Werner, *Phys. Rev. Lett.* **81**, 4132 (1998).
 - [16] R.M. Shelby, M.D. Levenson, and P.W. Bayer, *Phys. Rev. Lett.* **54**, 939 (1985).
 - [17] K. Bergman, H.A. Haus, E.P. Ippen, and M. Shirasaki, *Opt. Lett.* **19**, 290 (1994); C. Yu and H. Haus, private communication.

LIST OF FIGURES

FIG. 1. A schematic of the mechanism leading to amplitude squeezing in nonlinear fiber interferometers. (a) Amplitude dependent phase shift deforms the solitons' symmetrical coherent-noise distribution into a crescent-shaped distribution. (b) The auxiliary pulse is used to rotate the mean field relative to the crescent to allow maximum amplitude-noise reduction to be measured in direct detection.

FIG. 2. A schematic of the experimental setup. The shaded area highlights the components that form the Mach-Zehnder interferometer. HWP, half-wave plate; QWP, quarter-wave plate; PBS, polarizing beamsplitter; M, mirror. The inset shows a typical plot of the sum-photocurrent noise as the auxiliary-field phase is scanned; the bottom plot is obtained by fixing the phase to maximize the noise reduction. Both plots were obtained by averaging 5 time scans.

FIG. 3. Experimental quantum-noise reduction as a function of average power in the soliton arm (squared soliton number N^2). (a) 3.4 m of fiber, $T = (0.4 \pm 0.1)\%$; (b) 6.0 m of fiber, $T = (0.11 \pm 0.01)\%$ (triangles), $T = (0.32 \pm 0.01)\%$ (filled circles), $T = (1.0 \pm 0.4)\%$ (squares), and for clarity only one error bar for each data set is displayed; (c) 9 m of fiber, $T = (0.53 \pm .05)\%$. For all data the detection efficiency is 78%.

FIG. 4. Comparison of the experimental data, corrected quantum-noise reduction vs. the squared soliton number N^2 (diamonds), with numerical simulations: hollow squares refer to the case where the auxiliary pulse is in a coherent state and filled circles to the case where input quantum noise of the auxiliary pulse is propagated through the fiber; lines connecting the points are added for guidance. (a) 6.0 m of fiber, $T = (0.11 \pm 0.01)\%$ (experiment), $T = 0.1\%$ (simulations); (b) 6.0 m of fiber, $T = (0.32 \pm 0.1)\%$ (experiment) $T = 0.35\%$ (simulations); (c) 6.0 m of fiber, $T = (1.0 \pm 0.4)\%$ (experiment), $T = 1.0\%$ (simulations). In the inset in (a) shows a comparison of the theoretical results of Ref. [10] (down triangles) with the corrected experimental quantum-noise reductions (up triangles) in cases where the strong pulse is a fundamental soliton. The data points are for various fiber lengths with correspondingly different recombination ratios T .

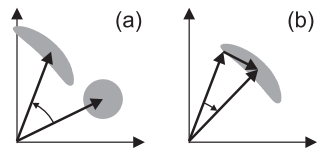


FIG. 1 M. Fiorentino et al “*Soliton squeezing...*”

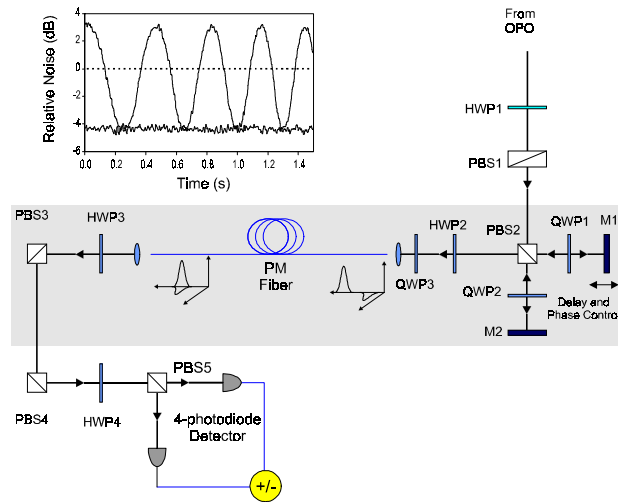


FIG. 2 M. Fiorentino et al “*Soliton squeezing...*”

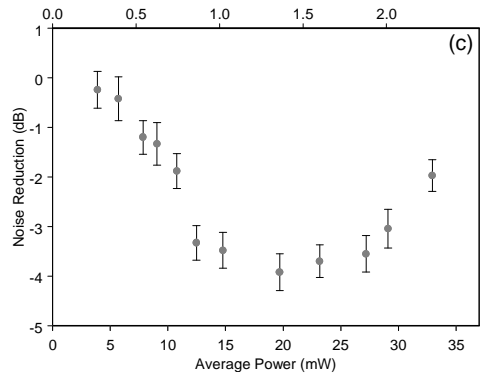
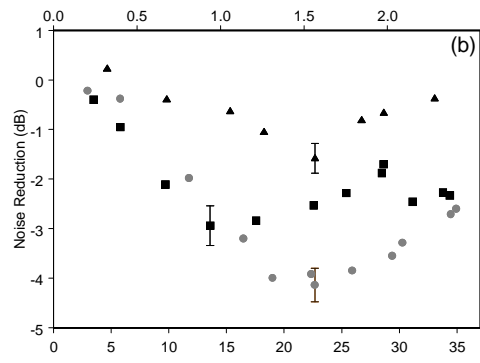
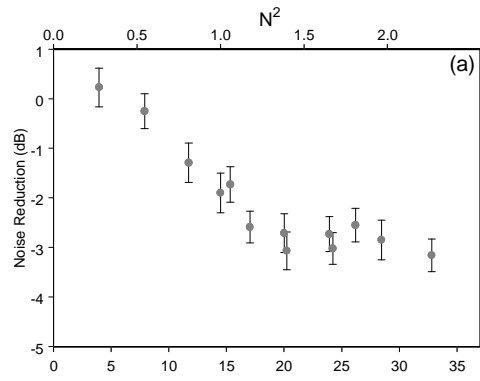


FIG. 3 M. Fiorentino et al “*Soliton squeezing...*”

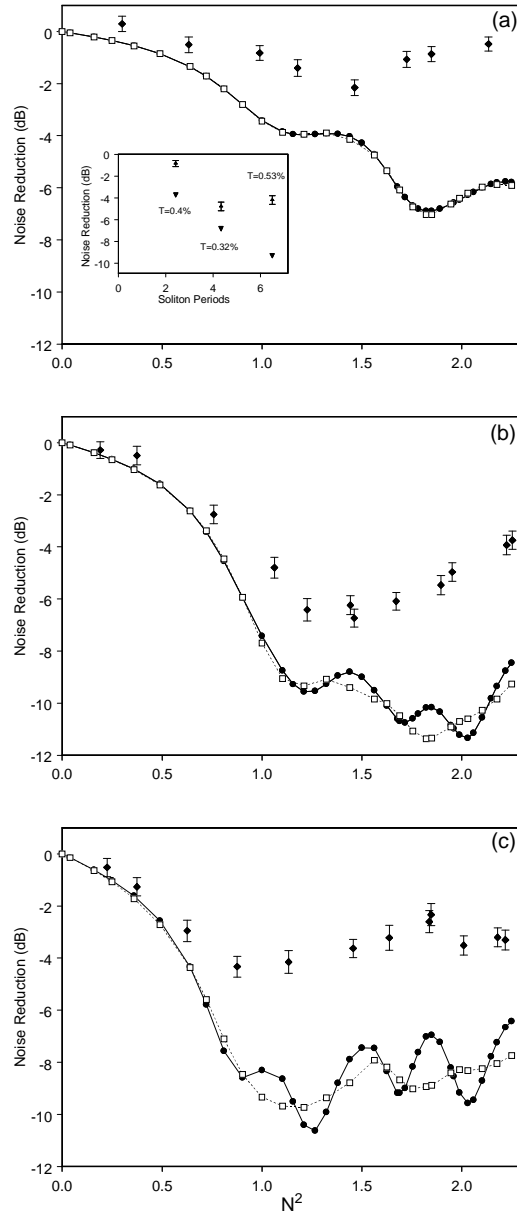


FIG. 4 M. Fiorentino et al “*Soliton squeezing...*”